Supersonic Winds in the Jovian Aurorae

Daniel Rego, Nicholas Achilleos*, Tom Stallard, Steve Miller[#],
Department of Physics and Astronomy, University College London,
Gower Street, London WC1E 6BT, U.K.

Renée Prangé,
Institut d'Astrophysique Spatiale, UMR-CNRS 120, Batiment 121,
Université de Paris XI,
91405 Orsay Cedex, France.
Michele Dougherty
Space and Atmospheric Physics, Imperial College, London SW7 2BZ, U.K.
and
Robert D. Joseph
Institute for Astronomy, University of Hawaii, Woodlawn Drive, Honolulu, Hawaii 96822, U.S.A.

*Nicholas Achilleos was a visiting astronomer on the NASA Infrared Telescope Facility, operated by the Institute for Astronomy, University of Hawaii, on behalf of NASA.

[#] To whom correspondence should be addressed.

Jupiter's magnetic field controls a region of space which extends some seven million kilometres, towards the sun, and all the way out to the orbit of Saturn. This giant magnetosphere couples to the planet's upper atmosphere producing million megawatt, circumpolar auroral emissions and delivering enough energy to keep local atmospheric temperatures hundreds of degrees warmer than expected. In turn, as the planet rotates, its magnetic field drags a dense, ionised, equatorial sheet of plasma, two million kilometres across, like a twirling ballerina's skirt. But how does this magnetosphere/atmosphere interaction work? Auroral electrojets - ion winds which race around Jupiter's auroral ovals - feature as a key component in theoretical models of how rotational energy can be transferred from Jupiter to the plasmasheet [1,2] and how winds may transport the auroral heating to lower latitudes [3-5]. But this vital link in the magnetosphere/atmosphere coupling has been missing, until now. Here we report the first direct evidence that auroral electrojets do exist, with wind speeds approaching or in excess of the speed of sound. Monitoring the electrojet can provide detailed information about the jovian magnetosphere/atmosphere coupling; modelling can now proceed on a firm empirical footing.

Jupiter's aurorae are some of the most energetic electromagnetic phenomena in the entire Solar System. Emitting up to 10^{13} Watts in the ultraviolet and infrared regions of the spectrum, they are between 100 and 1000 times more powerful than Earth's average aurorae (6,7). The high magnetospheric energy inputs needed to power such emissions cause significant local heating of the upper jovian atmosphere - the co-existing neutral thermosphere and electrically charged ionosphere. Detailed knowledge of how the ionosphere behaves is essential to understanding how this energy is distributed throughout the upper atmosphere and how it affects the chemistry there (3,4,8). Standard models of the jovian magnetic field have the plasmasheet, which is several jovian radii thick, extending from 5 jovian radii (R_J) (inside the orbit of Io, located at $5.9R_J$), and co-rotating with the planet out to ~20-30R_J, where co-rotation breaks down (9); many of the energetic particles which produce aurorae originate from here. According to Hill, corotation is enforced by a large scale current system which flows radially outwards in the plasmasheet, and closes by Birkeland (field-aligned) currents (upward from Jupiter nearer to Io's orbit, and downward from the more distant magnetosphere), and largely meridional Pedersen currents in the ionosphere (1). There, the magnetic and electric fields should result in anti-corotational (clockwise) ion winds (**E x B** Hall drift) - the electrojets; these flow along the oval(s) mapped onto the planet by the aurorally active magnetic field lines. These electrojets are also expected to frictionally accelerate the ambient neutral gas (5) and - together with other processes - to generate fast thermospheric winds needed to redistribute part of the auroral heating (4).

The magnetospheric Birkeland currents required by Hill's mechanism have indeed been detected (10), but there was only very indirect evidence for the mechanisms in the jovian ionosphere/thermosphere (11, 12). Our direct evidence for auroral electrojects is contained in high resolution infrared spectra obtained using the NASA Infrared Telescope Facility (IRTF) on Mauna Kea, Hawaii. These spectra were taken at 3.953μm, a wavelength sensitive to the H_3^+ molecular ion, on the night of August 8, 1997, using the IRTF facility spectrometer, CSHELL. Our

observations appear to have encompassed an "auroral event", maybe similar to those known in UV data (10,13-16).

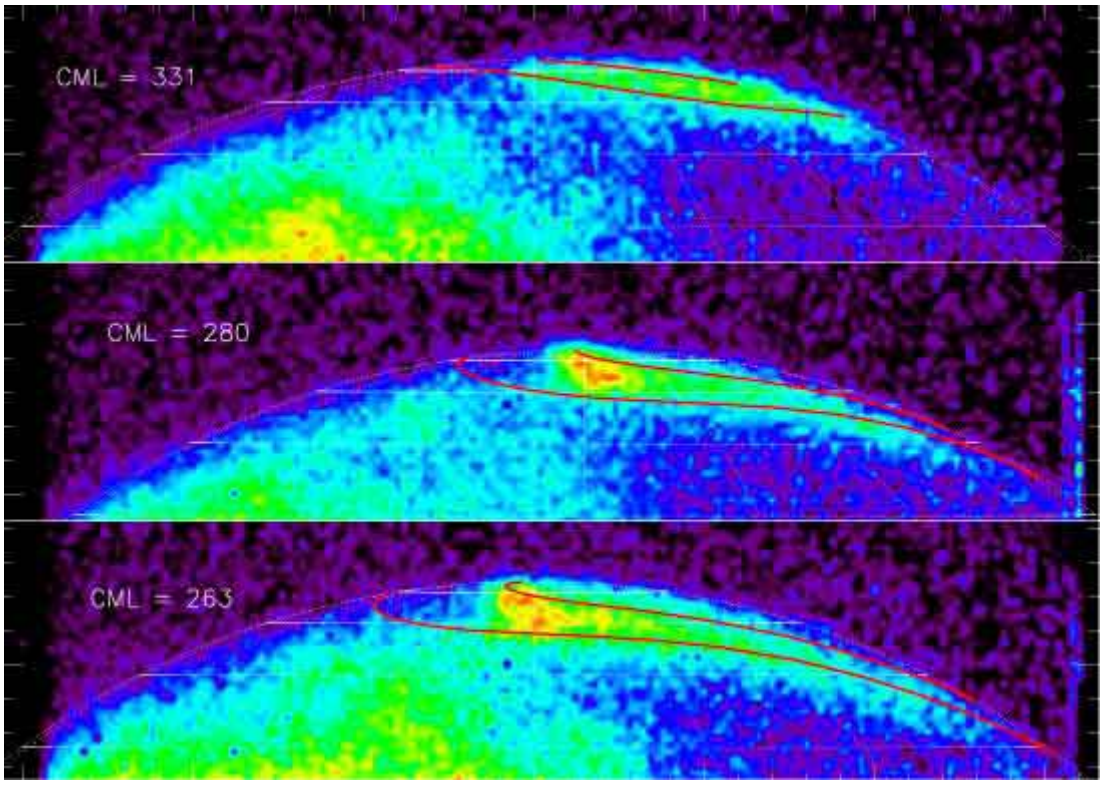

Figure 1: Series of CVF (1.4% spectral resolution) images taken of the northern auroral region, on August 8, 1997.
Bottom: 08:54U.T.; Middle: 09:22U.T.; Top: 10:46U.T.
Central wavelength: 3.953μm; exposure time: 5s; pixel scale: 0.2"; seeing: ~0.8"; tracking accuracy, ~0.1"/minute.
A planetary grid (white dotted lines: longitudinal divisions 18°; latitudinal divisions 10°), which includes the $30R_J$, (more poleward) and $5.9R_J$, (more equatorward) field line footprints from the most recent VIP4 jovian magnetic field model (7), has been fitted to the limb. Each division on the axes is 1", the width of the CSHELL slit used for the spectral images.
The bright emission lying along the magnetic field line footprints is due to the H_3^+ ν_2 $Q(1^-)$ line at 3.953μm; incident solar radiation at high latitudes is absorbed by jovian stratospheric methane. The bright emission seen on the body of the planet at lower latitudes is due to reflected solar IR: the shorter CH_4 column is insufficient to absorb all the incident radiation here. The central wavelength is not constant across the array when CSHELL is used in CVF mode, and this limits the use that can be made of our images to visualising the overall structure, rather than investigating the detailed morphology. The images show that both arcs are within the visible limb of the planet, and correspond approximately to the magnetic footprints shown.

CSHELL operates both as a long-slit spectrometer and as a direct imager with a pixel scale of 0.2 arcsec (corresponding to a linear distance at Jupiter of ~ 680km). Figure 1 shows a sequence of CVF images of the northern polar auroral region, taken on August 8, 1997. Unlike data taken at similar central meridian longitudes (CMLs) a year previously, which showed a single auroral arc, these images showed a double partial arc close to the footprints of the $30R_J$ (poleward) and 5.9 R_J (equatorward) magnetic field lines respectively (Fig. 1 bottom and middle panels). Our observations of the "double arc" event lasted about half an hour; two hours after our initial observation only a single auroral arc showed (Fig. 1 top).

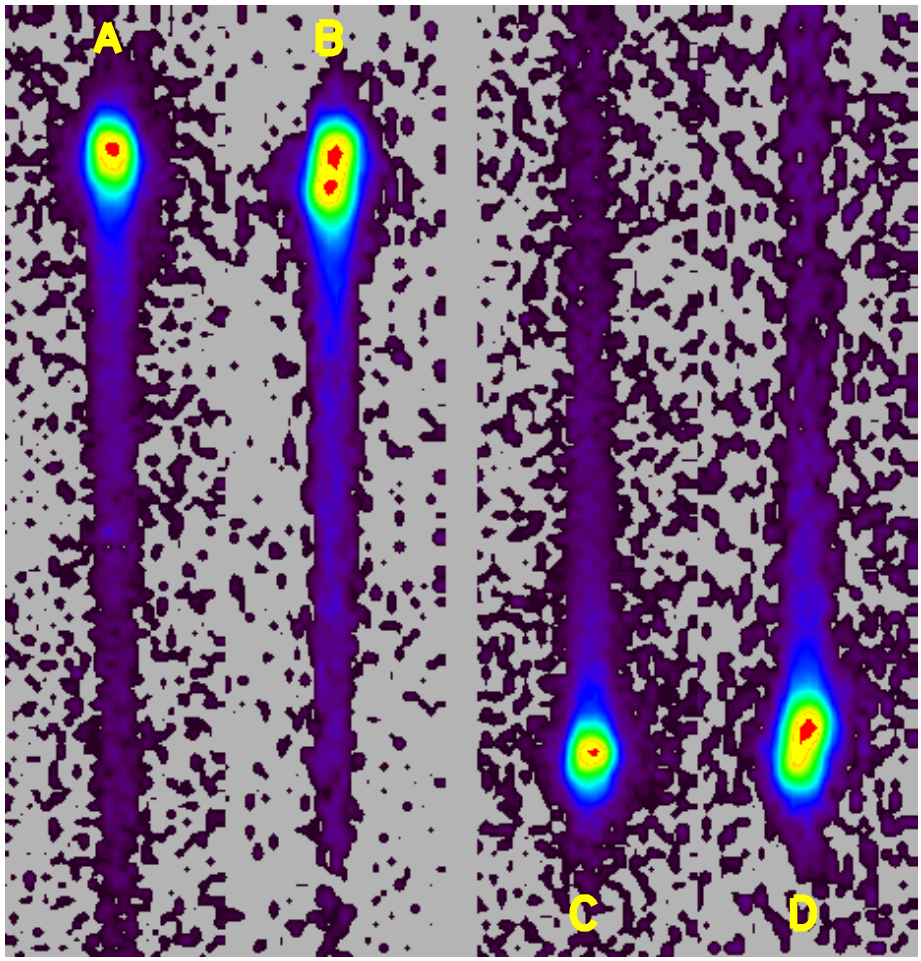

Figure 2: Comparison of CSHELL spectral images from 14 and 16 July, 1996, and 8 August, 1997.
These show the 1997 "two-peak" structure in the north and the "peak-tail" structure in the south, not visible in the 1996 data.
(A) 16 July, 1996, 09:56 UT. CML=248°. Northern Hemisphere.
(B) 8 August, 1997, 08:55 UT. CML=264°. Northern Hemisphere.
(C) 14 July, 1996, 08:46 UT. CML=264". Southern Hemisphere.
(D) 8 August, 1997, 09:05 UT. CML=270°. Southern Hemisphere.
The CSHELL 30"-long slit is set along the CML and the vertical axis indicates the position on the planet; north is at the top in the figure. The spectral images cover Jupiter from the poles - where the bright auroral emissions are located - to the equatorial regions, and each hemisphere is measured separately. The horizontal direction indicates wavelength (increasing left-to-right) for each of the four (A - D) spectral images shown. The spectral images have been flat-fielded to allow for the non-linear response of the array. Bad pixels have been removed. The central wavelength for each spectral image is 3.95301μm, corresponding to the rest wavelength of the H_3^+ ν_2 Q(1,0$^-$) line. The wavelength has been corrected for any slight non-alignment of the slit on the array and for variation in the wavelength calibration along the slit (total effect <1 pixel for the entire 150 pixel, 30", slit-length), using atmospheric emission lines at 3.95251μm and 3.95416μm; in the case of our data, no discernible systematic wavelength shift was observed.
The other "event" spectral images, listed in Table 1, show the same wavelength structure as B), for the northern hemisphere, and D), for the south. Post-event spectral images have the same structure as A), for the north, and C), for the south, i.e. they show neither the "double-peak" nor the "arc-tail" structure, nor any large or systematic wavelength shifts.

Table 1: Derived Line-of-Sight Velocity Shifts (8 August, 1997)

Time	CML	IP	OP	Diff.
(UT)			(km/s)	
During event				
08:50	260 N	1.0	-1.8	-2.8
08:55	265 N	0.9	-1.3	-2.2
09:05	270 S	-0.8	2.5	3.3
09:10	274 S	-1.0	2.0	3.0
09:18	278 N	0.0	-2.3	-2.3
09:24	282 N	0.3	-2.1	-2.4
09:33	287 S	-0.7	2.0	2.7
09:38	290 S	-1.0	1.5	2.5
	N average	0.6	-1.9	-2.5
	S average	-0.9	2.0	2.9
Post event.....				
10:38	327 N	0.2	-1.1	-1.3
10:42	333 N	0.0	-1.1	-1.1
10:55	337 S	-0.4	0.4	0.8
11:00	341 S	-0.6	0.2	0.8
11:12	347 N	0.6	-0.6	-1.2
11:16	350 N	0.1	-0.8	-0.9
11:24	355 S	-0.4	-1.2	-0.8
11:32	359 S	-0.2	-0.6	-0.4
	N average	0.2	-0.8	-1.0
	S average	-0.4	-0.3	0.1

Table caption: Table of derived wavelength (velocity) shifts of the inner (equatorward) peak (IP) and outer (poleward) peak/tail (OP) for pairs of spectra, and the difference (OP - IP) between them, for the Jovian auroral regions. The CML is given in System III longitude and the letter "N" or "S" denotes measurement of either the northern or southern auroral region. Pairs of spectra, obtained within 4 minutes elapsed time of one another, have been combined to improve statistics; UT times refer to the observation mid-time. Errors in the IP, OP and difference velocity shifts for individual spectra are 0.5km/s and for pairs of spectral images are ±0.3 km/s (see main text); the averages are subject to errors of ±0.2 km/s. After the event, the outer structures were not seen, and the velocity values refer to the maximum measured poleward of the main peak; this often refers to very low intensity emission, with signal-to-noise < 3, as against the event velocities which all refer to high intensity emission with S/N > 10.

Used in echelle spectrometer mode each wavelength pixel corresponds to a dispersion of 2.9 km/s; with the slit width of 1" (i.e. 5 pixels) used in this study, CSHELL has a spectral resolving power of 20,700 (14.4km/s) for a source which fills the slit. For the spectral images reported here (Figure 2 and Table 1), the slit was aligned along the central meridian from pole to equator in order to obtain latitudinal profiles of the planet's H_3^+ emission; since the CSHELL aperture spans only 30", northern and southern hemispheres were observed separately. Spectral images were obtained in pairs of 60-second integrations on the planet (and 60s on the sky, for background subtraction), and a four-minute total elapse time. Any necessary corrections to the wavelength scale were made by reference to sky emission lines whose wavelengths lay close to the H_3^+ line (Fig. 2 caption, 17).

Fig. 1 shows that at the time of our observations in the north, the CSHELL slit positioning meant that it cut both the partial arcs, and that it crossed the poleward arc, in particular, very close to the rising (eastern) ansa. The resulting H_3^+ latitudinal profiles showed a "double peak" structure (Fig. 2B) in comparison with the single peak seen in 1996 (Fig. 2A). In addition, the wavelength of the outer (poleward) peak was red-shifted by about 1 pixel, in comparison with the inner (equatorward) peak. In the south, the images showed an arc plus diffuse emission and the H_3^+ latitudinal profiles an "arc-tail" structure (Fig. 2D), not seen in 1996 (Fig. 2C). The images showed that the slit crossed the auroral arc near the setting (western) ansa; the southern "tail" was blue-shifted by about one pixel. This behaviour was repeated in eight pairs of spectra - four in the north and four in the south - taken between 8:50 and 9:38 U.T., which appear to have spanned our "auroral event", but absent in spectra taken after that time (Table 1).

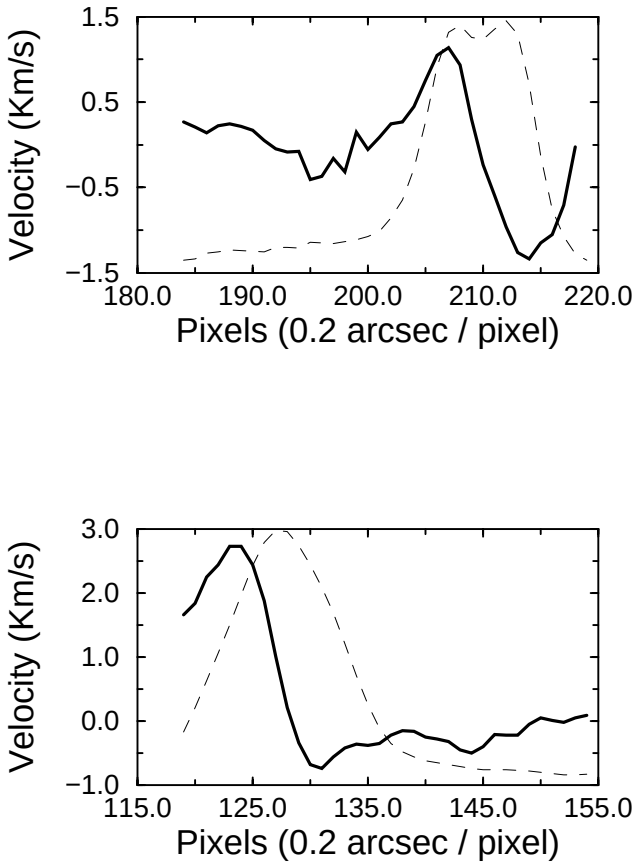

Figure 3: Line-of-sight velocity shifts and intensity profiles for the 1997 individual spectral images shown in Figure 1 for the H_3^+ ν_2 Q(1$^-$) line.
Planetary south is on the left and north on the right of the figure. Top panel: northern hemisphere CML 270°. Bottom panel: southern hemisphere CML 264°.
Velocities expressed as shifts from the planetary rest wavelength in km/s, determined from the wavelength of the main body of the planet, non-auroral emission, are shown as a solid line.
Systematic and fitting errors in our peak positions were determined by fitting the sky emission lines to a gaussian profile; these were shown to be +/-0.3km/s for five-pixel bins for the (relatively weak) sky lines on top of the bright sky continuum. The H_3^+ ν_2 Q(1,0$^-$) line was fitted for the sky-subtracted frames, so that the departure from gaussian profile caused by the adjoining sky lines and non-constant sky continuum was minimised.
The emission from the main body of the planet, from the equator to the sub-auroral latitudes is unaffected by Doppler shifts due to east-west winds, since the slit was positioned along the CML, giving a zero line-of-sight component. North-south wind speeds in the temperate to sub-auroral zones are <100 m/s (15), and

vertical velocities are even less. Thus this body-of-planet emission enables us to derive a planetary rest wavelength from which the shifts of the auroral peaks/tails can be measured.
Taking into account the error in fixing the planetary rest wavelength, each individual pixel velocity is subject to an error of ±0.5 km/s. The overplotted dashed line is the corresponding intensity (arbitary units). In both hemispheres, the outer intensity peak (northern hemisphere) or the tail (southern hemisphere), which corresponds approximately to the locus of the $30R_J$ field line, is associated with the greatest velocity shift, while the inner peak, corresponding approximately to the locus of the $5.9R_J$ (Io orbit) field line, is associated with a slight velocity shift in the opposite sense to the outer peak.

To measure the spectral shift in the 3.953μm H_3^+ line in the auroral regions, we fitted the intensity profile of the spectrum for each row of pixels with a gaussian in which the amplitude, half-width, central wavelength, and background were free parameters. To calibrate the wavelength in the jovian frame of reference, the H_3^+ line emitted on the body of the planet was measured on the same spectral images (see Fig. 2 caption). This planetary reference spectrum was obtained by summing the spectra along ~70 rows on the array (i.e. ~14") equatorward from the sub-auroral regions. Spectral shifts of the auroral emission peaks for those spectral images which exhibited the double-peak or peak-tail structure are given in Table 1, along with the results for the spectral images obtained just after the double-peaked structures disappeared. For each spectrum with a signal-to-noise ratio greater than 10, i.e. for all of the spectra in the auroral and near-auroral regions, the fitting procedure gives peak positions to an accuracy of ±0.1 pixels or ±0.3 km/s. Since the error is the same in fitting the profile on the body of the planet, the uncertainty in determining the shifts between either peak and the planetary rest wavelength is approximately ±0.5 km/s. Typical velocity profiles for the auroral regions are shown in Figure 3.

For the period when the two-peaked structure was present, Table 1 shows that in the northern auroral zone, the poleward peak is seen to have a mean redshift, relative to the peak 1" toward the equator, of -2.5 ±0.2 km/s. For the southern auroral zone, the relative blueshift between the equatorward peak and the poleward tail is +2.9 ±0.2 km/s. In each hemisphere, part of this relative shift is due to shifting of the equatorward peaks (+0.6km/s in the north, -0.9km/s in the south). After the two-arced structure disappeared, spectra from the limb of the planet showed shifts of -1 ±0.2 km/s in the north and +0.1 ±0.2 km/s in the south, with respect to the single auroral peak - effectively zero spectral shift in the south, and a small residual shift in the north.

Placing a point source asymmetrically in the slit could produce an apparent wavelength shift. But a detailed examination of this effect (17), making use of both images and spectra, ruled it out for the following reasons:
a) The images showed emission extended along the two arcs in the east-west direction for considerably more than 1", the width of the CSHELL slit; and, taking the northern images shown in Figures 1 for instance, there was some intensity variation in the east-west direction. But a slit positioning which put the brightest part of the poleward arc on one side of the slit and that of the lower latitude arc on the other side would have actually produced a relative blueshift for the outer peak, in contrast to what was observed;

b) The same spectral shifts were obtained for four spectral images in each of the northern and southern hemispheres, despite offsetting the telescope several times, over a period when Jupiter rotated much more than one slit width. The likelihood of producing such consistent wavelength shifts as a result of an essentially randomised positioning of point sources in the slit seemed negligible.

Thus our observations are consistent with H_3^+ ions flowing in a clockwise - anti-corotational - direction along the ~30 R_J auroral ovals in both hemispheres, as predicted by Hill (1) to enforce the co-rotation of the magnetospheric plasmasheet, and - with lower velocities - near the ~5.9 R_J auroral ovals in the opposite direction. This is more unexpected but Morgan et al. (18) have proposed currents flowing radially *towards* Jupiter in the plasma-sheet for about 0.2R_J inward of Io's orbit (a dense region called the "ribbon") to explain "auroral hiss" measured by Voyager. Such currents would drive counter-clockwise ionospheric winds, and may therefore explain the shifts which appear to be associated with our inner (~5.9R_J) peaks.

The speed of sound in the thermosphere in the region where H_3^+ is formed is 2.6 km/s (8). Since we detect only ~70% of the wind speed along the ~30 R_J ovals, our velocities in Table 1, corrected for the line-of-sight, indicate that the ion flows are close to the speed of sound or supersonic. The highest line-of-sight-corrected velocities are 3.3±0.4 km/s for the north outer peak and 3.6±0.4 km/s for the south "tail," with averages of 2.7±0.3 km/s and 2.9±0.3 km/s respectively. This detection of near-to-supersonic electrojets provides **both** the first direct evidence that high-velocity winds do exist in the jovian thermosphere/ionosphere **and** a powerful confirmation of our present understanding of the jovian magnetosphere and the ionospheric current systems it produces.

References

1. Hill, T.W., Inertial limit on corotation. *J. Geophys. Res*. 84, 6554-6558 (1979).

2. Hill, T.W., Dessler, A.J., & Goertz, C.K., Magnetospheric models, in *Physics of the Jovian Magnetosphere*, ed. Dessler, A.J., pp. 353-394 (1983).

3. Atreya, S.K., Ionospheres, in *Atmospheres and ionospheres of the Outer Planets and Their Satellites*. (Heidelberg: Springer-Verlag, 1986), 107-134.

4. Waite, J.H. Jr. *et al*., Electron precipitation and related aeronomy of the jovian thermosphere and ionosphere. *J. Geophys. Res.*, **88**, 6143-6163 (1983).

5. Sommeria, J., Ben Jaffel, L. & Prangé, R., On the existence of supersonic jets in the upper atmosphere of Jupiter. *Icarus*, **119**, 2-25 (1995).

6. Livengood, T.A., Moos, W.A., Ballester, G.E. & Prangé, R., Jovian ultraviolet auroral activity, 1981-1991. *Icarus*, **97**, 26-45 (1992).

7. Lam, H.A. *et al*., A baseline spectroscopic study of the infrared auroras of Jupiter. *Icarus*, **127**, 379-393 (1997).

8. Achilleos, N. *et al*., JIM: a time-dependent, three-dimensional model of Jupiter's thermosphere and ionosphere. *J. Geophys. Res (Planets)*., **103**, 20089-20112 (1998).

9. Connerney, J.E.P., Magnetic fields of the outer planets. *J. Geophys. Res*. **98**, 18,659-18,679 (1993).

10. Dougherty, M., Dunlop, M., Prangé, R. and Rego, D., Correspondance between field-aligned currents observed by Ulysses and Hubble Space Telescope auroral emission. *Planet. Space Sci.,* **46**, 531-540 (1998).

11. Prangé, R. *et al*., Detection of self-reversed Lyman-α lines from the jovian aurorae with the Hubble Space Telescope. *Astrophys. J.*, **484**, L169-173 (1997).

12. Miller, S. *et al*., Mid-to-low latitude H_3^+ emission from Jupiter. *Icarus*, **130**, 57-67 (1997).

13. Prangé, R. *et al*., Correlated variation of u.v. and radio emission during an outstanding auroral event. *J. Geophys. Res*., **98**, 18779-18792 (1993).

14. Gérard, J.C. *et al*., A remarkable auroral event observed in the ultraviolet with the Hubble Space Telescope. *Science*, **266**, 1975-1678 (1994).

15. Ballester, G.E. *et al*., Time-resolved observations of Jupiter's far-ultraviolet aurora. *Science*, **274**, 409-413 (1996).

16. Prangé, R. and Livengood, T.A., Monitoring jovian auroral activity, in *Ultraviolet Astrophysics Beyond the IUE Final Archive*, **ESA SP-413**, 29-36 (1998).

17. A detailed description of our data analysis is obtainable by anonymous ftp to jonny.phys.ucl.ac.uk; change directory to the pub/aurwinds/referees directory and download the .ps files there.

18. Morgan, D.D., Gurnett, D.A., Kurth, W.S. & Bagenal, F., The source of jovian auroral hiss observed by Voyager 1. *J. Geophys. Res*., **99**, 21213-21224 (1994).

19. Clarke, J.T. *et al*., HST far-ultraviolet imaging of Jupiter during the impacts of Comet Shoemaker-Levy 9. *Science*, **267**, 1302- 1307 (1995).

20. Dinelli, B.M. *et al*., UKIRT observations of the impact and consequences of Comet Shoemaker-Levy 9 on Jupiter. *Icarus*, **126**, 107- 125 (1997).

Acknowledgments

It is a pleasure to acknowledge the helpful assistance of staff at the NASA IRTF. In particular, we should like to thank the CSHELL support astronomer Dr. John Rayner for help in dealing with issues related to CSHELL. This work was supported by a grant from the UK Particle Physics and Astronomy Research Council.